Modelling Erythroctye Central Metabolism Informs Parasitic Drug Development

Yusuf Turhan

Contents

1. Abstract 1
2. Introduction 1
3. Materials and Methods 2
4. Results 4
4.1. Model building 4
4.2. Parameter estimation 4
4.3. Time course analysis 5
4.4. Steady state analysis 5
4.5. Metabolic Control Analysis 5
4.6. Model Robustness 7
4.7. Parameter Identifiability Analysis 8
4.8. Range Expansion 9
5. Discussion 11
6. Supplementary resources 12
7. References 12
8. Supplementary figures 14

1. Abstract

A model for erythrocyte central metabolism is created, which consisted of glucose transporter and reactions of glycolysis. It was shown to be robust to changes in a limited parameter value range, with some values more identifiable than others. The flux controlling reactions were determined, where hexokinase had a positive control and ATP hydrolysis had a negative control. The lack of flux control by glucose transport gives insight on anti-parasitic drug development, and the negative flux control of ATP hydrolysis possibly sheds light on autocatalytic nature of glycolysis. Lastly, it has been noted that model fitting with expanded parameter lower and upper bounds lead to suffering robustness and parameter identifiability, which may be fixed with longer parameter estimation runs.

2. Introduction

Erythrocytes are the constituent cells of human blood. They are essential to life as they deliver oxygen from lungs to faraway tissues and collect carbon dioxide (Corrons et al., 2021). Erythrocytes are also infection targets of parasites such as *Plasmodium falciparum* (Paul et al., 2015); hence, it is important to identify differences between erythrocyte metabolism and parasite metabolism for developing anti-parasitic drugs with little adverse effects to the host red blood cells. In this context, our aim with this project is to identify most critical reactions in erythrocyte metabolism, which can be adversely affected by anti-parasitic drugs.

The central metabolism of erythrcoytes mainly consists of the steps of glycolysis (Wijk & Solinge, 2005). Glucose is taken up by GLUT1 transporters, energy-investment reactions process glucose into high energy metabolic intermediates and energy-extraction reactions produce ATP molecules. In most other cells, reduced NADH produced by these reactions are used for ATP production, however, as

mature erythrocytes lack mitochondria (Wijk & Solinge, 2005), NADH is oxidized back to NAD+ by reducing pyruvate to lactate, which is then exported out of the cell.

Another important distinction of erythrocyte glycolysis is Rapoport-Luebering Shunt (Wijk & Solinge, 2005). These reactions bypass one of the energy producing steps in glycolysis to produce an intermediate called 2,3-bisphosphoglycerate (2,3-BPG), which plays an important role in regulating oxygen affinity of hemoglobulin.

3. Materials and Methods

COPASI version 4.44 Build 295 (Hoops et al., 2006) was used to build and run our models. Reaction velocity formulas used are listed in Supplementary Table 1. Steady state metabolite concentrations and reaction fluxes for parameter estimation were obtained from Joshi & Palsson (1990). R version 4.3.3 was used for the visualizations not done with COPASI.

As for the experimental data, steady state concentrations of G6P(0.038mM), F6P(0.016mM), F1,6BP(0.0076mM), DHAP(0.14mM), GA3P(0.0067mM), 1,3PG(0.004mM), 3PG(0.045mM), 2PG(0.014mM), PEP(0.017mM), Pyruvate(0.077mM), ADP(0.27mM), ATP(1.5mM) and steady state flux for hexokinase (0.000311mM/s) were obtained from Joshi & Palsson (1990). Additionally, Glucose concentration(5mM) were added to the experimental variables as it was the expected steady state intracellular concentration in an erythrocyte (Loyola-Leyva et al., 2022).

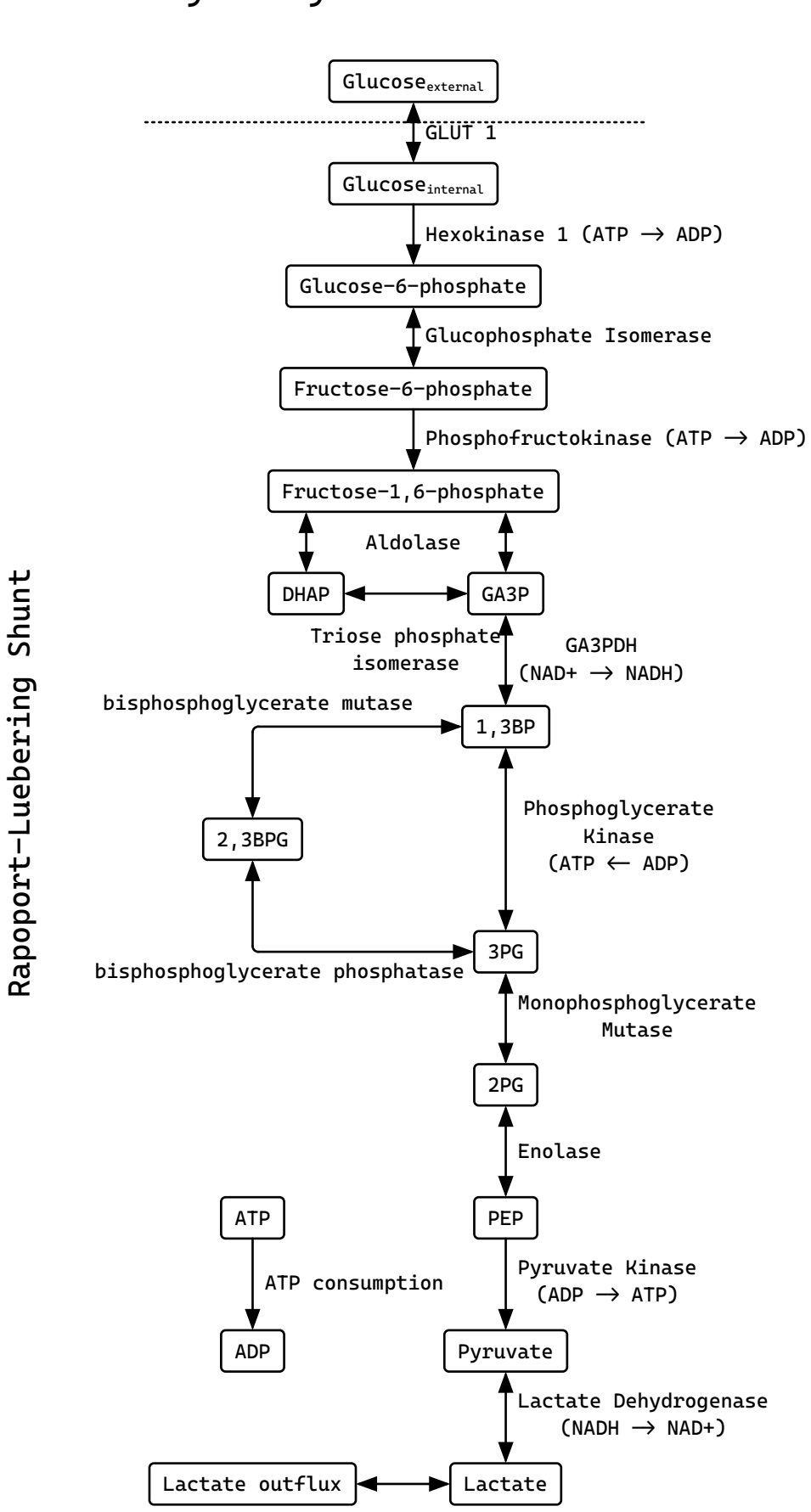

Figure 1: Erythrocyte central metabolism.

4. Results

An array of different models with differing complexity were created in our erythrocyte modelling group. I will be reporting the creation and findings of the most basic model in here.

4.1. Model building

This model includes the GLUT1 facilitative diffusion transporter, reactions of glycolysis, and energy expenditure function and a pyruvate outflux function. It does not take rapaport luebering shunt or lactate dehydrogenase into account. The reactions of our model are detailed in Supplementary Table 2. The reaction parameters found on the literature are reported in Supplementary Table 3. Other reaction parameters were estimated in Section 4.2. The species starting concentrations were specified as 1.6 mM for ATP (Pospieszna et al., 2021), 0.2 mM for ADP (Pospieszna et al., 2021), and 5mM for Glucose (Loyola-Leyva et al., 2022). All other species' starting concentrations were set to 0mM.

4.2. Parameter estimation

To save time while prototyping different model builds, steady state was achieved during parameter estimation step. All the parameters that are not defined in Supplementary Table 3 were added to the parameter estimation. Experimental data is also set at this step. For the parameters to be estimated, lower bounds were set to 10^{-2} and upper bounds were set to 10^{2}. Then, parameter estimation was run with the particle swarm algorithm with iteration limit at 150, swarm size 100 and standard deviation 10^{-6}. The parameter estimation results can be seen in Figure 2. ADP and ATP steady state concentrations were the hardest parameters for the optimization algorithm to fit.

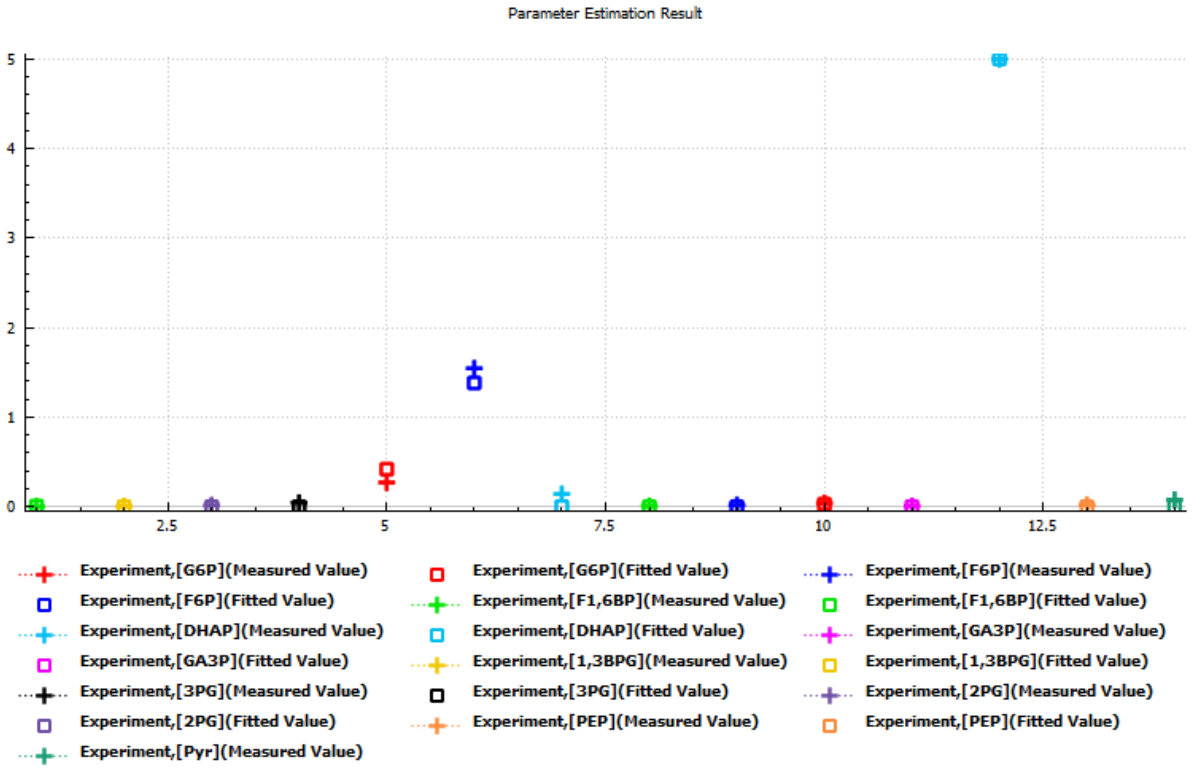

Figure 2: Parameter estimation results

4.3. Time course analysis

After the steady state achievement in the parameter estimation step, a time course analysis can be done to show the kinetics of our model adjusted to achieve steady state that fits our data. For visualization purposes, internal glucose concentration was set to 0 mM and a time course analysis was run, which can be seen in Figure 3.

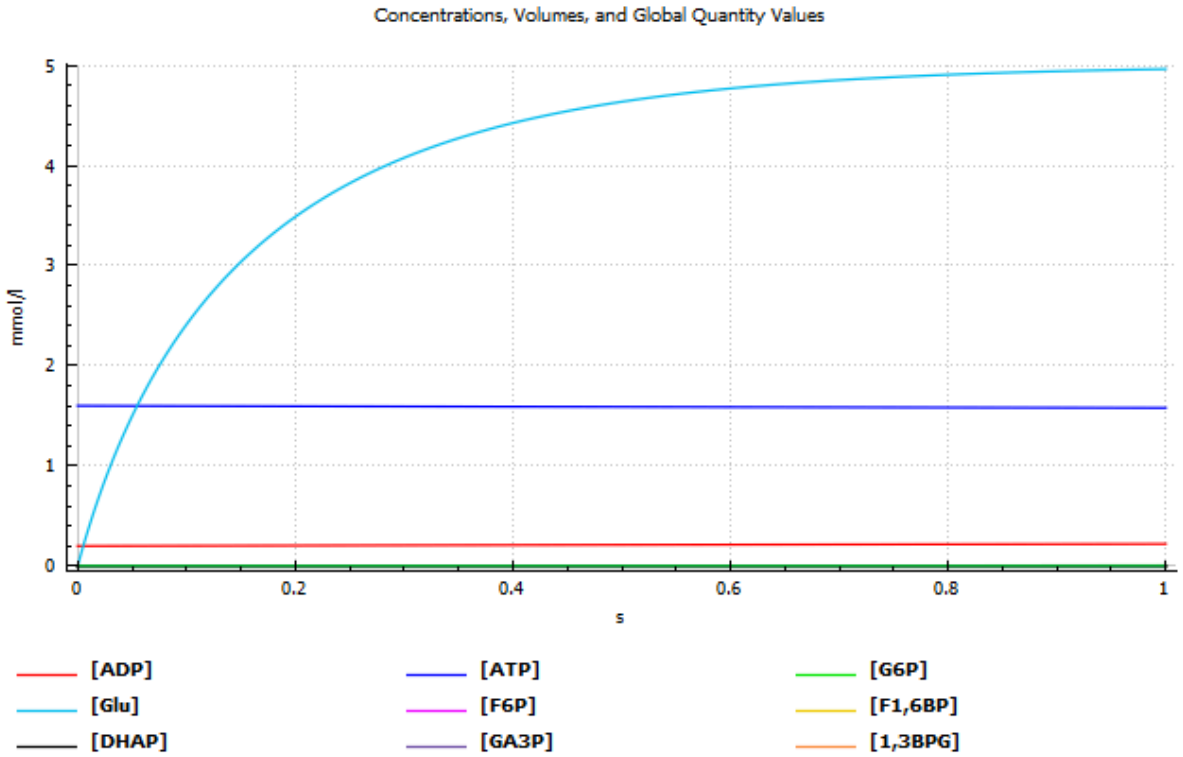

Figure 3: Time course analysis of our model when the internal glucose concentration is set to 0 mM

4.4. Steady state analysis

A steady state achievement can be deduced by inspecting the time course analysis, but it is better to run a steady state analysis and report the results. Steady state reaction fluxes can be found at Supplementary Table 4 and steady state species concentrations can be found at Supplementary Table 5.

4.5. Metabolic Control Analysis

To identify reaction controlling steps that can be affected by anti-parasitic drugs, we can perform a Metabolic Control Analysis(MCA) and inspect the flux control coefficients of the reactions in our model. As shown in Figure 4, reaction fluxes are controlled positively by Hexokinase(Glu -> G6P), and controlled negatively by Energy expenditure(ATP -> ADP).

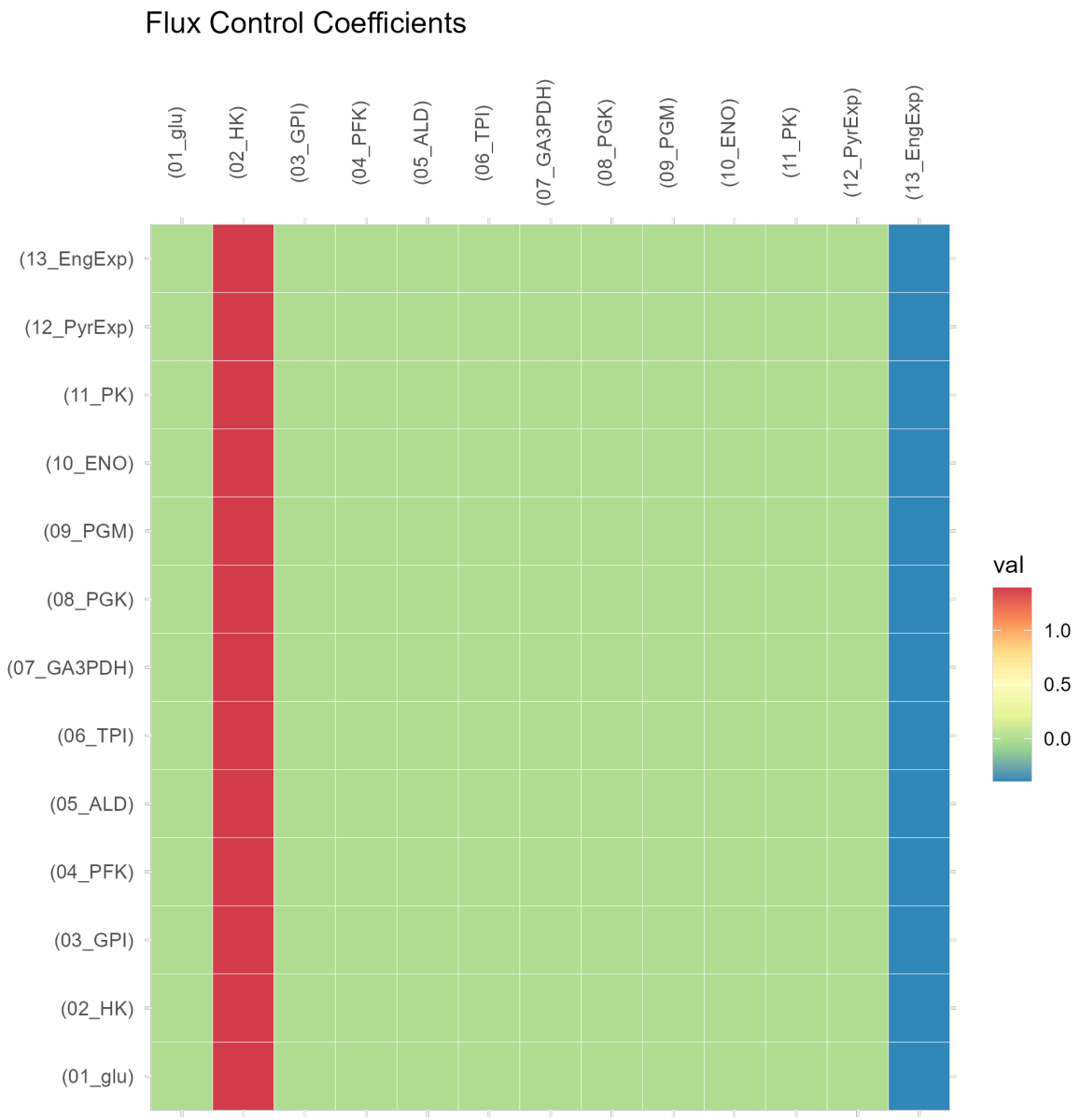

Figure 4: Metabolic Control Analysis results showing that the reaction fluxes are controlled positively by Hexokinase and negatively by Energy Expenditure.

4.6. Model Robustness

In order to test the robustness of our model, which would mean the ability of our model to behave similarly under different parameter estimation runs, we have run the parameter estimation for 10 times. The resulting fits were plotted in the Figure 5.

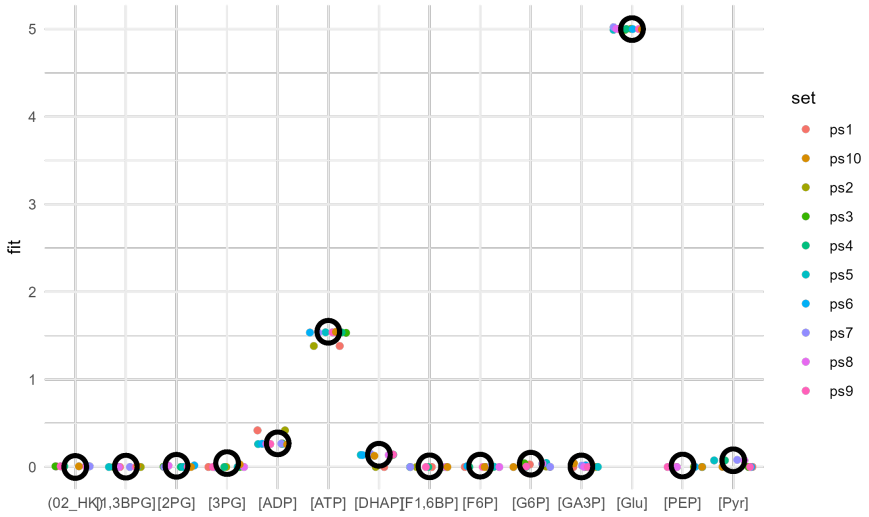

Figure 5: Parameter estimation step is repeated to test robustness and parameter identifiability. Black circles represent the target experimental values, and the colored dots represent different parameter sets fitted. ATP and ADP steady state concentratios were the main hurdles for fitting.

Then, MCA analyses for the parameter sets obtained from these parameter estimation runs were plotted in Figure 6. We see that all the parameter sets plotted show the same flux control coefficients as our initial MCA. This shows that our model is robust to different parameter estimation runs at parameter ranges 10^{-2}-10^{+2}.

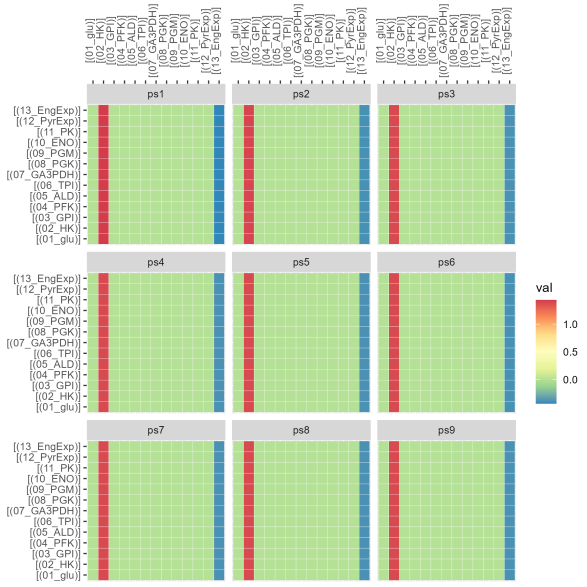

Figure 6: Multiple MCA comparison plot shows that in all parameter sets, reaction fluxes controlled positively by Hexokinase and negatively by Energy Expenditure.

4.7. Parameter Identifiability Analysis

The parameter sets obtained during Section 4.6 were used to test the identifiability of our model parameters that were not defined with values from the literature search. When we plot the variability of these parameters in Figure 7, some parameters show little variablity, meaning they are more identifiable, and some parameters show high variability, meaning they are less identifiable. Interestingly, some parameters, particularly V_{max} of Hexokinase and k_1 of Energy expenditure, which were also the controlling steps, had their values in a very small range near the lower bounds of the parameter estimation range at 10^{-2}. This has prompted us to perform a range expansion and repeat the parameter estimations, and test the robustness and parameter identifiability again.

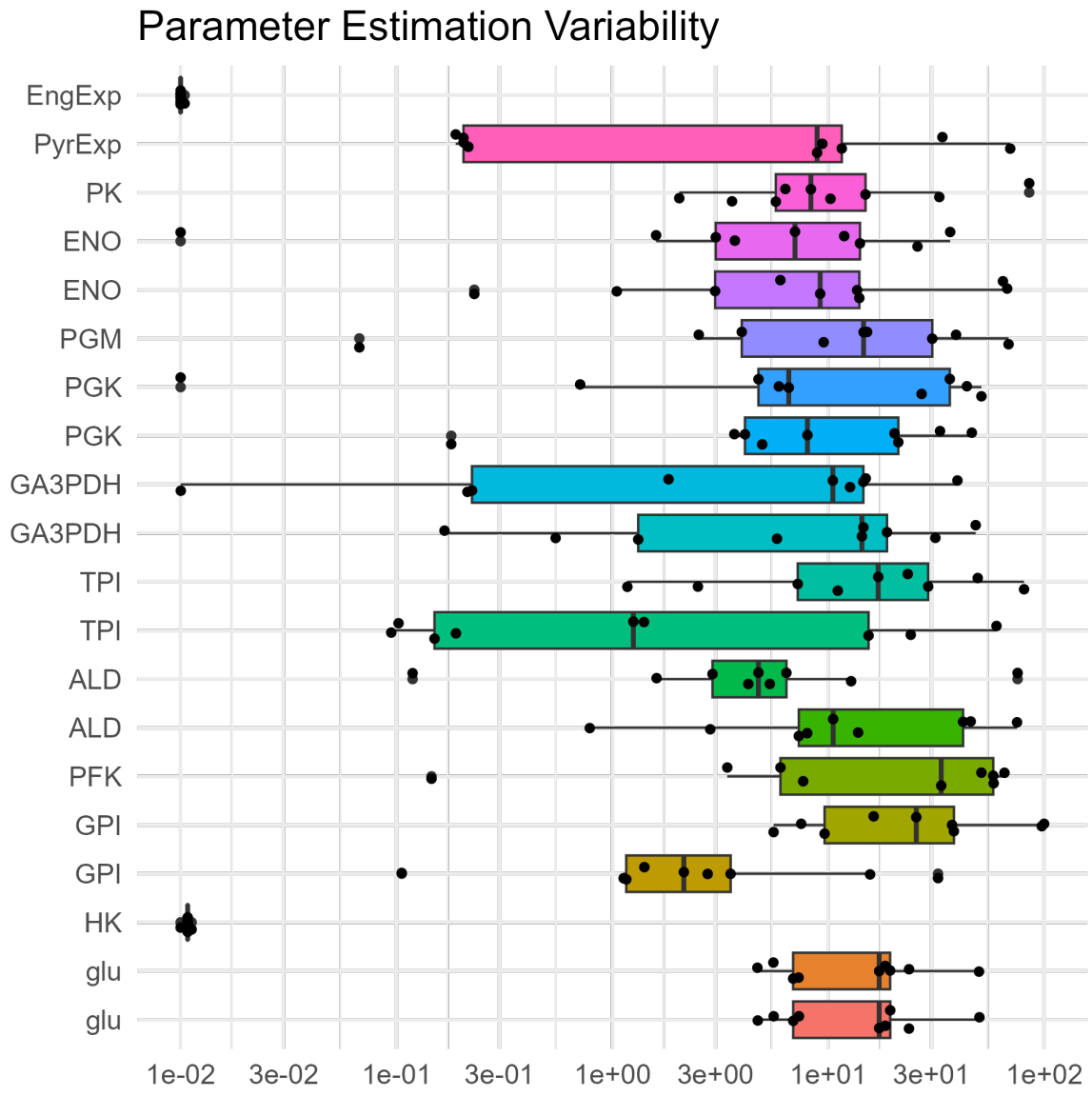

Figure 7: To determine parameter identifiability, parameter values from the parameter estimation runs were plotted. We can see they show differing variation, and the more variable parameters are less identifiable. As some parameters showed very little variation at the lower bound of the parameter estimation range, we have decided to perform range expansion.

4.8. Range Expansion

Lower and upper bounds for estimation of our non-defined parameters are expanded to −90% and +900% of their latest fit values. Then, 10 independent parameter estimation steps are done. Figure 8 shows that, for three runs, parameter estimation were not able to fit the ADP and ATP steady state concentrations. This may mean optimization algorithms cannot find global minima in a reasonable time in the range-expanded solution space.

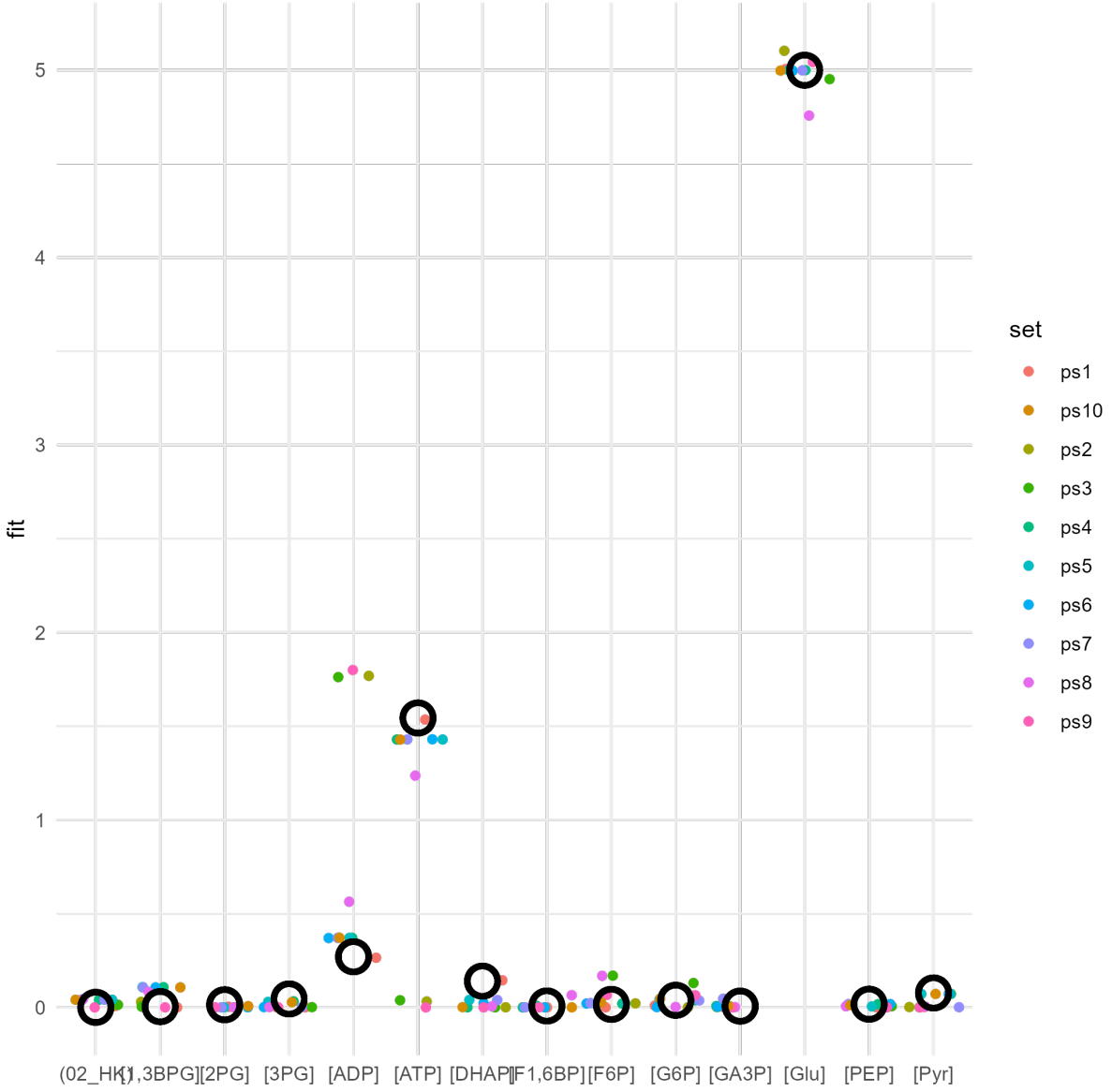

Figure 8: Parameter fits for different parameter sets in range-expansion runs. ATP and ADP were harders to fit, and three runs were not able to fit those steady states, showing inverted fits with respect to these experimental measurements.

We then wanted to see whether our model is still robust to different estimated parameter sets in the expanded ranges. Multiple MCA comparison for the range-expansion parameter sets shown in Figure 9 surprises us with only one MCA showing meaningful fluxes. Which means that our model is not robust at the range-expanded parameter space.

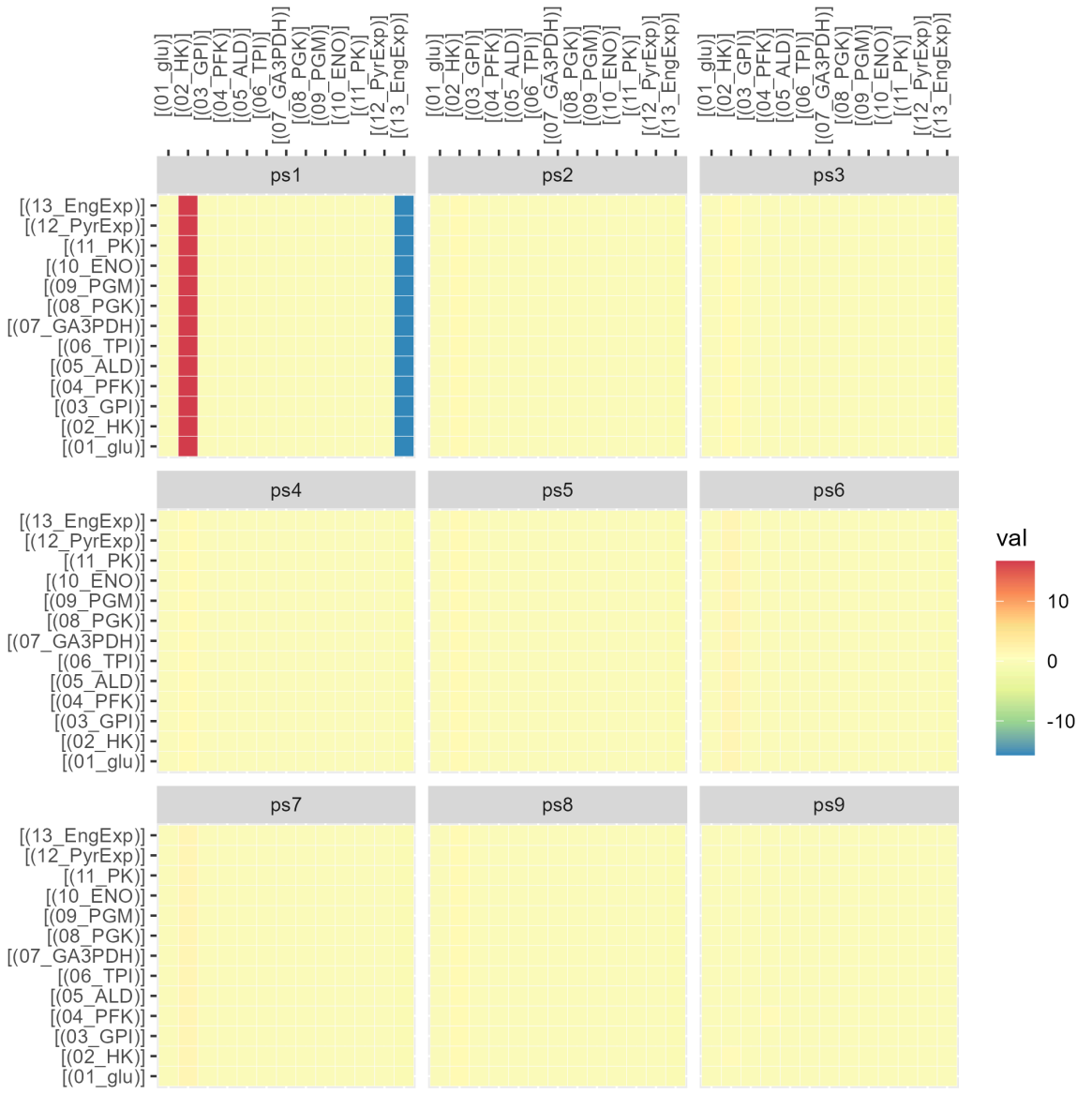

Figure 9: MCA comparison for the 9 parameter sets estimated with range expansion. Except for the first parameter set, all other show near-zero fluxe control coefficients.

Plotting the estimated parameter variability plot again for range expansion in Figure 10 shows a much different picture compared to range-limited runs. Parameter variations and means are much more inconsistent with each other and the previous range-limited figures, possibly due to incomplete fitting due to increased parameter space in range-expansion.

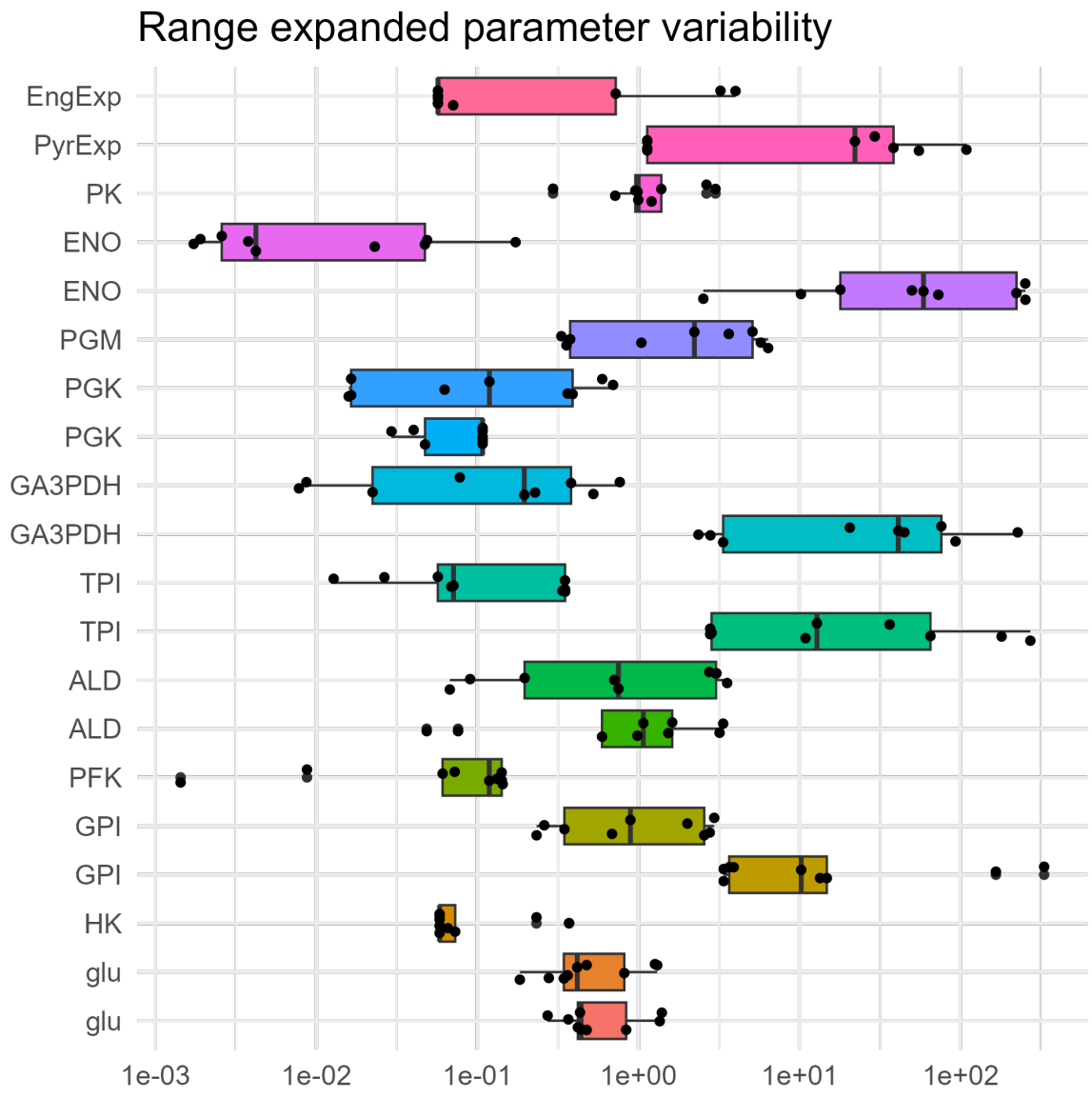

Figure 10: Distribution of parameters in range-expanded parameter estimation runs.

5. Discussion

Although this model was designed to be as simple as possible, we believe it holds some valuable insight into the erythrocyte glycolysis. It was able to model Hexokinase as a positive controller of reaction fluxes, but not glucose transporter. This results agree with the other, more sophisticated models in our group. This fact is important for drug development against parasites as it has been seen that in parasites such as *Plasmodium falciparum*, glucose transporter is seen as the most important reaction that needs to be targeted for inhibition (Niekerk et al., 2016)

Another flux controlling reaction captured by our model is the Energy Expenditure. It negatively controls the reactions fluxes, and it is most likely caused by the autocatalytic nature of ATP in glycolysis. In other words, if ATP is converted to ADP in a high rate, there will be less ATP to be used by upstream reactions, slowing reaction fluxes.

The autocatalytic activity may also play a role in the phenomenone seen in Figure 8, where failed parameter estimation runs were not able to fit ATP and ADP steady state concentrations.

We have also shown that, in the narrow window of parameter ranges defined in our initial parameter estimations, our model is robust to changes in different parameter runs, being able to fit the experimental values all the time and giving the same flux control coefficients in MCA. The estimated parameters in these runs also showed similar values (Figure 7). However, Hexokinase and Energy Expenditure related reaction parameters were clustered with a low variation near the lower bounds defined. For this reason, a parameter range expansion was performed and new parameter estimations were run. Some of these runs were not able to fit ADP and ATP, and most of them showed near-zero reaction flux control coefficients in their MCA. The parameter variability was much different compared to previous runs as well (Figure 10). This may be due to the expanded parameter space, where the optimizers did not run long enough to fit the parameters. To resolve this hypotheses, more parameter estimation runs with longer iteration should be made.

For future research, our model can be expanded with drug simulation experiments. The reaction rates of some reactions in our model such glucose transporter can be artifically inhibited, simulating some anti-parasitic drugs.

6. Supplementary resources

The model, data files, and R code for plots can be found at https://github.com/yusufozgur/Modelling-Erythrocyte-Central-Metabolism

7. References

Corrons, J. V., Casafont, L. B., & Frasnedo, E. F. (2021). Concise review: how do red blood cells born, live, and die?. *Annals of Hematology*, *100*(10), 2425–2433. https://doi.org/10.1007/s00277-021-04575-z

Gorovits, N., & Charron, M. J. (2003). What we know about facilitative glucose transporters: Lessons from cultured cells, animal models, and human studies. *Biochemistry and Molecular Biology Education*, *31*(3), 163–172. https://doi.org/10.1002/bmb.2003.494031030227

Hoops, S., Sahle, S., Gauges, R., Lee, C., Pahle, J., Simus, N., Singhal, M., Xu, L., Mendes, P., & Kummer, U. (2006). COPASI—a COmplex PAthway SImulator. *Bioinformatics*, *22*(24), 3067–3074. https://doi.org/10.1093/bioinformatics/btl485

Ikura, K., NARITA, H., SASAKI, R., & CHIBA, H. (1978). Immunochemical and Enzymatic Properties of Bisphosphoglyceromutase/phosphatase and Phosphoglyceromutase from Human Erythrocytes. *European Journal of Biochemistry*, *89*(1), 23–31. https://doi.org/10.1111/j.1432-1033.1978.tb20892.x

Joshi, A., & Palsson, B. O. (1990). Metabolic dynamics in the human red cell. Part IV—Data prediction and some model computations. *Journal of Theoretical Biology*, *142*(1), 69–85. https://doi.org/10.1016/s0022-5193(05)80013-x

Loyola-Leyva, A., Alcántara-Quintana, L. E., Terán-Figueroa, Y., & González, F. J. (2022). In vitro effect of high glucose concentrations on erythrocyte morphology assessed by scanning electron microscopy. *Micron*, *154*, 103179. https://doi.org/10.1016/j.micron.2021.103179

Mulquiney, P. J., & Kuchel, P. W. (1999). Model of 2, 3-bisphosphoglycerate metabolism in the human erythrocyte based on detailed enzyme kinetic equations: equations and parameter refinement. *Biochemical Journal*, *342*(3), 581–596. https://doi.org/10.1042/bj3420581

Niekerk, D. D. van, Penkler, G. P., Toit, F. du, & Snoep, J. L. (2016). Targeting glycolysis in the malaria parasite Plasmodium falciparum. *FEBS J.*, *283*(4), 634–646.

Paul, A. S., Egan, E. S., & Duraisingh, M. T. (2015). Host–parasite interactions that guide red blood cell invasion by malaria parasites. *Current Opinion in Hematology*, *22*(3), 220–226. https://doi.org/10.1097/moh.0000000000000135

Pietkiewicz, J., Gamian, A., Staniszewska, M., & Danielewicz, R. (2009). Inhibition of human muscle-specific enolase by methylglyoxal and irreversible formation of advanced glycation end products. *Journal of Enzyme Inhibition and Medicinal Chemistry*, *24*(2), 356–364. https://doi.org/10.1080/14756360802187679

Pospieszna, B., Kusy, K., Slominska, E. M., & Zieliński, J. (2021). Life-long sports engagement enhances adult erythrocyte adenylate energetics. *Scientific Reports*, *11*(1). https://doi.org/10.1038/s41598-021-03275-y

Ryzlak, M. T., & Pietruszko, R. (1988). Heterogeneity of glyceraldehyde-3-phosphate dehydrogenase from human brain. *Biochimica Et Biophysica Acta (BBA) - Protein Structure and Molecular Enzymology*, *954*, 309–324. https://doi.org/10.1016/0167-4838(88)90086-6

Stocchi, V., Magnani, M., Canestrari, F., Dachà, M., & Fornaini, G. (1982). Multiple forms of human red blood cell hexokinase. Preparation, characterization, and age dependence. *J. Biol. Chem.*, *257*(5), 2357–2364.

Wijk, R. van, & Solinge, W. W. van. (2005). The energy-less red blood cell is lost: erythrocyte enzyme abnormalities of glycolysis. *Blood*, *106*(13), 4034–4042. https://doi.org/10.1182/blood-2005-04-1622

8. Supplementary figures

Supplementary Table 1: Biochemical reaction velocity formulas used in our model.

Name	Formula
Mass action (irreversible)	$\mathrm{k1}\ [S]$
Michealis-Menten (irreversible)	$V_{\max}\frac{[S]}{K_m + [S]}$
Michealis-Menten (reversible)	$\frac{V_f \frac{[S]}{K_{\mathrm{ms}}} - V_r \frac{[P]}{K_{\mathrm{mp}}}}{1 + \frac{[S]}{K_{\mathrm{ms}}} + \frac{[P]}{K_{\mathrm{mp}}}}$
Uni-Bi (reversible)	$\frac{V_f\left(\frac{[A]}{K_{\mathrm{ma}}}\right) - V_r\left(\frac{[P]}{K_{\mathrm{mp}}}\right)\left(\frac{Q}{K_{\mathrm{mq}}}\right)}{1 + \left(\frac{[A]}{K_{\mathrm{ma}}}\right) + \left(\frac{[P]}{K_{\mathrm{mp}}}\right) + \left(\frac{[Q]}{K_{\mathrm{mq}}}\right) + \left(\frac{[P][Q]}{K_{\mathrm{mp}}K_{\mathrm{mq}}}\right)}$
Bi-Bi (irreversible)	$\frac{V_{\max}\frac{[A]}{K_{\mathrm{ma}}}\frac{[B]}{K_{\mathrm{mb}}}}{1 + \frac{[A]}{K_{\mathrm{ma}}} + \frac{[B]}{K_{\mathrm{mb}}} + \frac{[A][B]}{K_{\mathrm{ma}}K_{\mathrm{mb}}}}$
Bi-Bi (reversible)	$\frac{v_f * \left(\frac{A}{K_{\mathrm{ma}}}\right) * \left(\frac{B}{K_{\mathrm{mb}}}\right) - v_r * \left(\frac{P}{K_{\mathrm{mp}}}\right) * \left(\frac{Q}{K_{\mathrm{mq}}}\right)}{1 + \left(\frac{A}{K_{\mathrm{ma}}}\right) + \left(\frac{B}{K_{\mathrm{mb}}}\right) + \left(A * \frac{B}{K_{\mathrm{ma}} * K_{\mathrm{mb}}}\right) + \left(\frac{P}{K_{\mathrm{mp}}}\right) + \left(\frac{Q}{K_{\mathrm{mq}}}\right) + \left(P * \frac{Q}{K_{\mathrm{mp}} * K_{\mathrm{mq}}}\right)}$

Supplementary Table 2: Reactions that are defined in our model.

Name	Reaction	Rate Law
Glucose influx	Glu0 = Glu	Michealis-Menten (reversible)
Hexokinase	Glu + ATP -> G6P + ADP	Bi-Bi (irreversible)
Glucose-6-Phosphate Isomerase	G6P = F6P	Michealis-Menten (reversible)
Phosphofructokinase	F6P + ATP -> F1,6BP + ADP	Bi-Bi (irreversible)
Aldolase	F1,6BP = DHAP + GA3P	Uni-Bi (reversible)
Triosephosphate Isomerase	DHAP = GA3P	Michealis-Menten (reversible)
Glyceraldehyde-3-Phosphate Dehydrogenase	GA3P = 1,3BPG	Michealis-Menten (reversible)
Phosphoglycerate kinase	1,3BPG + ADP = 3PG + ATP	Bi-Bi (reversible)
Phosphoglucomutase	3PG = 2PG	Michealis-Menten (reversible)
Enolase	2PG = PEP	Michealis-Menten (reversible)
Pyruvate Kinase	PEP + ADP -> Pyr + ATP	Bi-Bi (irreversible)
Pyruvate expenditure	Pyr ->	Mass action (irreversible)
Energy Expenditure	ATP -> ADP	Mass action (irreversible)

Supplementary Table 3: Reaction parameters found in the literature.

Reaction	Parameter	Value	Reference
Glucose Influx	Km	1mM	(Gorovits & Charron, 2003)
Hexokinase	K_{mGLU}	0.046 mM	(Stocchi et al., 1982)
Hexokinase	K_{mATP}	0.6 mM	(Stocchi et al., 1982)
Glucose-6-Phosphate Isomerase	K_{mG6P}	0.445 mM	sabio 21894
Glucose-6-Phosphate Isomerase	K_{mF6P}	0.063 mM	sabio 21899
Phosphofructokinase	K_{mF6P}	0.045 mM	46778
Phosphofructokinase	K_{mATP}	0.12 mM	46779
Aldolase	$K_{\mathrm{mF1,6BP}}$	0.007 mM	(Mulquiney & Kuchel, 1999)
Aldolase	K_{mDHAP}	2 mM	(Mulquiney & Kuchel, 1999)
Aldolase	K_{mGA3P}	1 mM	(Mulquiney & Kuchel, 1999)
Triosephosphate Isomerase	K_{mDHAP}	1.5 mM	12716
Triosephosphate Isomerase	K_{mGA3P}	0.55 mM	12715
Glyceraldehyde-3-Phosphate Dehydrogenase	K_{mGA3P}	0.1 mM	(Ryzlak & Pietruszko, 1988)
Glyceraldehyde-3-Phosphate Dehydrogenase	$K_{\mathrm{m1,3BPG}}$	0.01 mM	(Ryzlak & Pietruszko, 1988)
Phosphoglycerate kinase	$K_{\mathrm{m1,3BPG}}$	0.0025 mM	24923
Phosphoglycerate kinase	K_{mADP}	0.099 mM	24920
Phosphoglycerate kinase	K_{m3PG}	0.6 mM	24927
Phosphoglycerate kinase	K_{mATP}	0.32 mM	24924
Phosphoglucomutase	K_{m3PG}	0.1 mM	(Ikura et al., 1978)
Enolase	K_{m2PG}	0.2 mM	(Pietkiewicz et al., 2009)
Enolase	K_{mPEP}	0.58 mM	(Pietkiewicz et al., 2009)
Pyruvate Kinase	K_{mPEP}	0.15 mM	2365
Pyruvate Kinase	K_{mADP}	0.091 mM	2370

Supplementary Table 4: Steady state reaction fluxes

Reaction	Flux (extensive) [mmol/s]	Flux (intensive) [mmol/(l*s)]
Glu + ATP -> G6P + ADP	0.000767727	0.000767727
G6P = F6P	0.000767727	0.000767727
F6P + ATP -> F1,6BP + ADP	0.000767727	0.000767727
F1,6BP = DHAP + GA3P	0.000767727	0.000767727
DHAP = GA3P	0.000767727	0.000767727
GA3P = 1,3BPG	0.001535455	0.001535455
1,3BPG + ADP = 3PG + ATP	0.001535455	0.001535455
3PG -> 2PG	0.001535455	0.001535455
2PG = PEP	0.001535455	0.001535455
PEP + ADP -> Pyr + ATP	0.001535455	0.001535455
Pyr ->	0.001535455	0.001535455
ATP -> ADP	0.001535455	0.001535455
Glu0 = Glu	0.000767727	0.000767727

Supplementary Table 5: Steady state concentrations

Name	Concentration [mmol/l]	Rate [mmol/(l*s)]	Transition Time [s]
ADP	0.26454544	−4.38E-16	86.14564277
ATP	1.53545456	4.38E-16	500
G6P	5.85E-06	3.19E-19	0.007621794
Glu	4.984964034	1.37E-14	6493.144329
F6P	5.65E-07	−2.13E-19	0.000736095
F1,6BP	4.75E-07	−4.25E-19	0.000618081
DHAP	0.091506739	4.55E-17	119.1917247
GA3P	4.31E-06	4.25E-19	0.002805583
1,3BPG	3.20E-08	5.31E-18	2.08E-05
3PG	7.51E-07	−4.89E-18	0.000488982
2PG	3.00E-06	2.13E-19	0.001950586
PEP	4.38E-07	1.06E-18	0.000285009
Pyr	5.05E-05	−1.28E-18	0.032894088